# Silicon implanted with carbon ions: SiC crystallite formation and strain in Si

F. Eichhorn, N. Schell, W. Matz, R. Kögler
Forschungszentrum Rossendorf, Institute of Ion Beam Physics and Materials Research

Carbon is a common impurity in CZ-silicon crystals. C in Si can deteriorate important device characteristics as leakage current and minority carrier lifetime, if the C concentration exceeds a threshold of about $1x10^{19}$ C/cm$^3$ [1]. On the other hand an additional C ion implantation into Si reduces the transient enhanced diffusion of B dopants [2] and can improve device characteristics because of the suppression of the formation of extended defects after implantation [3]. Moreover, high energy C implantation is applied for the formation of gettering layers with high trapping efficiency against unwanted metal impurities [4]. Furthermore, SiC is well known as a wide-band gap semiconductor with high thermal and chemical stability for realizing integrated circuits for high frequency, high power and high temperature applications [5]. C implantation with stoichiometric doses at elevated temperatures (400 - 900°C) [6] or an implantation followed by annealing [5], [7] is used to synthesize buried SiC layers in Si.

The aim of this paper is to investigate the process of the formation of SiC precipitates in the Si matrix during C implantation. It is known from previous investigations that SiC formation is not a single step process [8], [9], [10]. Depending on the conditions of mixing C into Si the carbon is localized in different atomic surroundings. By implantation of C into Si the damaged and implanted region is in a non-equilibrium state and most of the C atoms occupy interstitial positions. In thermodynamic equilibrium the solubility for C in Si is only $10^{-3}$ to $10^{-4}$ at.% at 1200 to 1400°C [11] and the excess C is dissolved substitutionally or the new phase SiC is formed. The volume concentration of C and with it the strain of the Si substrate lattice varies in depth; resulting in different local conditions for nucleation and growth of Si-C complexes and SiC particles. The present study is focused on the strain in the crystalline material (Si substrate and SiC particles) due to implantation and on the first stages of forming the SiC phase in the Si lattice by using X-ray diffraction with synchrotron radiation. The new material research goniometer of the ROBL beamline at the ESRF [12] enables to follow the early stage of phase formation.

The samples were prepared by implantation of C ions with an energy of 195 keV into Si (001) wafers under perpendicular incidence, at doses varying from $5x10^{15}$ ions/cm$^2$ to $4x10^{17}$ ions/cm$^2$ and temperatures between room temperature and 800°C. A survey of the samples is given in Table 1.

**Tab. 1:** Sample characterization: Concentration of C, implantation temperature and ion fluence

| Maximum C concentration ($10^{21}$ atoms/cm$^3$) | Percentage of stoichiometric concentration for SiC | Implantation temperature (°C) | Ion fluence ($10^{16}$ ions/cm$^2$) |
|---|---|---|---|
| 0.27 | 0.6 | room temp. | 0.5 |
| 0.27 | 0.6 | 500 | 0.5 |
| 0.27 | 0.6 | 800 | 0.5 |
| 2.7 | 6 | 500 | 5 |
| 22 | 45 | 500 | 40 |
| 22 | 45 | 800 | 40 |

X-ray diffraction using synchrotron radiation was carried out on the ROBL beamline at the ESRF Grenoble [12]. In ROBL the X-ray beam is conditioned by adaptively bent Si mirrors and a Si(111) - Si(111) double crystal monochromator. The choosen wavelength was $\lambda$ = 0.10008 nm.

During the implantation process in the near-surface layer the ions generate only weak distortions (damage profile). Later the ions are stopped in a deeper region (ion distribution

profile), resulting in a higher content of impurity atoms (implants) with their deformation field. The damage and ion distribution profiles calculated with TRIM and a schematic representation of the regions are shown in Fig. 1. In dependence on the process temperature, the local implant concentration and the strain values determine the formation of a solid solution of C in Si, a substitutional alloy, or crystallites of SiC.

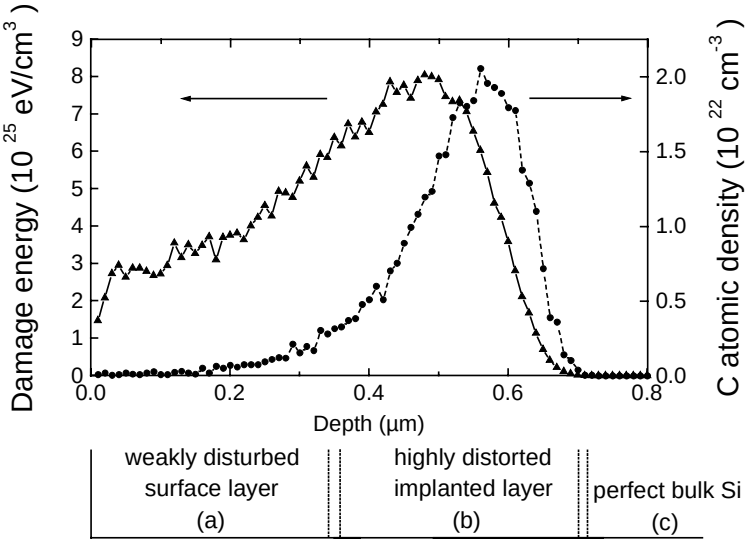


**Fig. 1:** Depth distribution of damage energy and C atoms after implantation of $4x10^{17}$ $cm^{-2}$ C ions with an energy of 195 keV into Si(100) as calculated by the TRIM code (version 96.01). The regions of different strain for the simulation model are indicated.

The formation of SiC crystallites is indicated by the reflections (111), (200), (220), and (311) of the 3C-SiC phase. Other SiC polytypes were not detected in the X-ray diffraction diagram. The reflections (111), (220), (311), and (400) of the Si substrate were used to characterize the damage and strain of the Si lattice in dependence on the implanted ion dose and the thermal treatment. Both, the damage and the ion distribution profile influence the X-ray diffraction peaks from silicon due to the strain induced by them in the formerly perfect Si lattice.

Fig. 2 shows the diffraction patterns in the vicinity of the most intense 3C-SiC(111) reflection which is representative to detect the SiC formation. No signal caused by SiC crystallites smaller than 3 nm was detected after implantation with the lowest dose of $5x10^{15}$ ions/$cm^2$. With increasing implantation dose ($5x10^{16}$ ions/$cm^2$ to $4x10^{17}$ ions/$cm^2$) and temperature (500 °C to 800 °C) carbon related diffraction intensities occur starting with a broad distribution at the low-angle side and growing up to a crystalline peak at the expected line position.

The high resolution diffraction curves of the Si(400) reflection are given in Fig. 3. They reveal a lattice strain component perpendicular to the sample surface. The occurence of fringes beside the interference maximum is characteristic for a layered structure. The diffraction line is a superpositon of intensity modulations caused by the weakly distorted surface layer as well as by the implanted layer. The later varies in density and strain as graded transitions from the surface layer to the matrix. To get quantitative results for strain and layer thickness the measured intensity versus scattering angle is simulated by the HRXRD-code [13] with a model on the base of the damage and ion distribution profiles. The near-surface region (a) of the Si wafer is only weakly distorted by the ion damage. In the deeper region (b) near the maximum of the damage and the implant concentration the Si lattice is destroyed in a higher degree resulting in an X-ray peak shift. In the depth the bulk material (c) diffracts X-rays as a perfect crystal. The superpositon of the waves diffracted by the bulk material (c) and by the weakly distorted near-surface region (a) causes X-ray

interference fringes, so far as the phase shift is only small. If these fringes are visible the lattice strain in the near-surface region can be assumed to be zero for modelling.

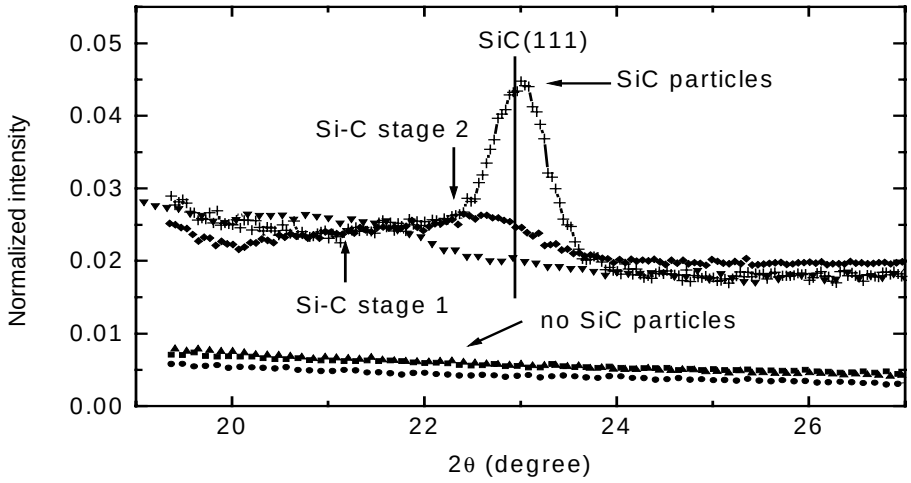


**Fig. 2:** Diffraction curves (θ:2θ scans) in the vicinity of the most intense 3C-SiC(111) reflection indicating the formation of Si-C prestages and crystalline SiC particles.
Curves correspond to different implantation conditions:
■ $5x10^{15}$ ions/cm$^2$ at room temperature, ● $5x10^{15}$ ions/cm$^2$ at 500°C
▲ $5x10^{15}$ ions/cm$^2$ at 800°C, ▼ $5x10^{16}$ ions/cm$^2$ at 500°C,
◆ $4x10^{17}$ ions/cm$^2$ at 500°C, + $4x10^{17}$ ions/cm$^2$ at 800°C.
The line marks the position of the SiC(111) diffraction line according to the JCPDS-PDF data. For clearness the curves are shifted vertically in two groups.

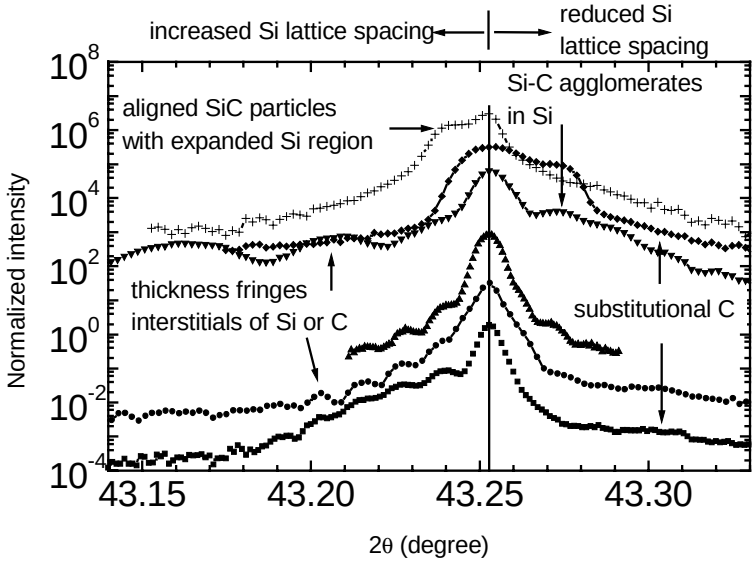


**Fig. 3:** Diffraction curves (θ:2θ scans) of the Si(400) reflection revealing the lattice strain component perpendicular to the sample surface. Characteristic features and their cause are marked (Symbols as in Fig. 2). For clearness the curves are shifted vertically by multiplying neighbouring curves by 10.

At the lowest fluence of $5x10^{15}$ C ions/cm$^2$ the silicon lattice is expanded due to implantation. Above the non-implanted substrate region a strained layer with a thickness in the range of 100 ... 200 nm and a strain on the order of $1x10^{-3}$ due to the interstitials of C and/or Si exists as it is indicated by the extended intensity left from the substrate peak (marked by the vertical line in Fig. 3). This strained layer is located below a non-strained Si layer with a thickness of 500 nm which causes the thickness fringes. This layer thickness

increases up to 560 nm with increasing implantation temperature. Again all the samples implanted with $5x10^{15}$ ions/cm$^2$ show very similar curves. At the high-angle tail of the Si(400) reflection a small peak is detected which indicates the existence of a Si lattice region with reduced spacing ($(\Delta d/d)_{Si}$ = -0.001). At the higher implantation dose of $5x10^{16}$ C ions/cm$^2$ the fringe distance increases which means that the thickness of the undisturbed layer is reduced to 120 nm. Its transition to the implant layer is more smooth. At the doses $5x10^{16}$ ions/cm$^2$ and $4x10^{17}$ ions/cm$^2$ some additional peaks appear in the vicinity of the main peak.

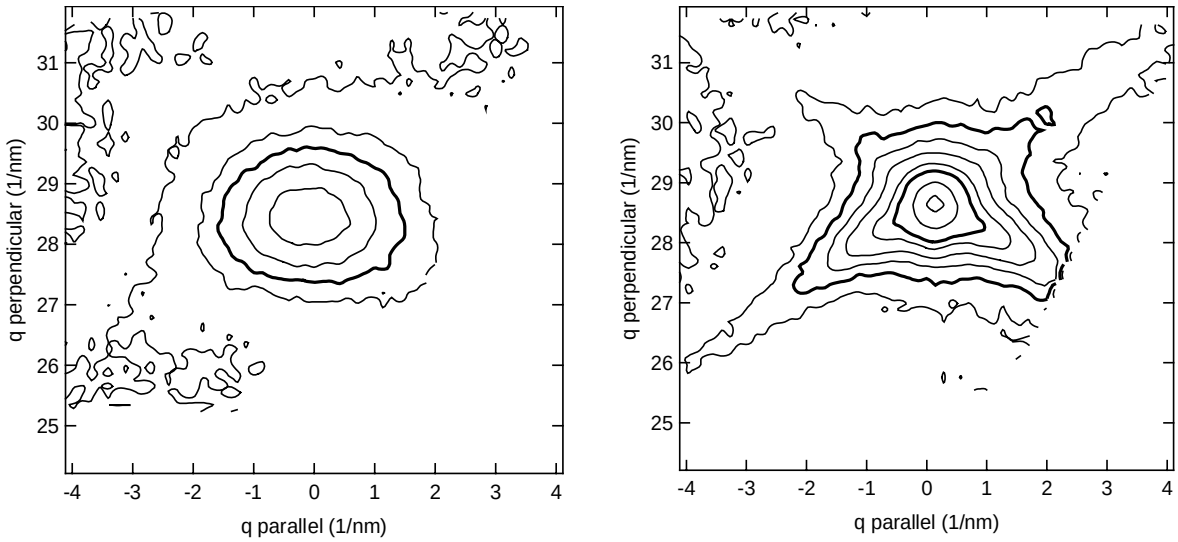


**Fig. 4:** Reciprocal space maps near the SiC(002) reflection for Si wafers implanted with $4x10^{17}$ cm$^{-2}$ C$^+$ with an energy of 195 keV at 500 °C (on the left) or 800 °C (on the right), respectively. The isointensity lines are choosen in a logarithmic scale, the bulk ones corresponds to 512 counts and 2048 counts per 3 sec.

In addition, the orientation relation between the lattice of the SiC particles and the Si matrix is determined by the measurement of reciprocal space maps (RSM) of symmetric SiC(002) - Si(004) and asymmetric SiC(113) – Si (113) reflection pairs. The alignment of the cubic axes of the SiC crystallites to the Si matrix is confirmed. Fig. 4 shows the RSM near the SiC(002). The centre of the Si(004) reflection lies at $q_{||}$=0 and $q_{\perp}$=46.3 nm$^{-1}$. For implantation at the lower temperature of 500 °C the cubic axes of the SiC crystallites are orientated with a nearly isotropic spread (FWHM ≈ 4.5°) parallel to Si [001] direction.
More of SiC grows during carbon implantation at 800°C and a more complex distribution is found (right hand side of Fig. 4): The majority of crystallites is highly aligned with a spread of 2.5° isotropically distributed around [001] as shown by the symmetric top of the SiC peak, whereas the minority is anisotropically distributed around this axis with preferences into the <111> directions (streaks at the bottom of the SiC peak).

The experimental observations can be explained with the following processes:

1. The observed Si lattice expansion at the fluence of $5x10^{15}$ C ions/cm$^2$ is caused mainly by carbon interstitials and Si self-interstitials. No SiC precipitates, which X-rays detect as crystalline, were found (see Fig. 2, 3).

2. The Si lattice region with reduced spacing ($()d/d)_{Si}$ = -0.001) may be caused by substitutional C with an average concentration of $1.5x10^{20}$ atoms/cm$^3$ according to Vegard's rule. The corresponding peak is detected up to the dose of $5x10^{16}$ C ions/cm$^2$ at 500°C.

3. Very small SiC particles (pre-stages 1 and 2) with enhanced lattice spacings ($()d/d)_{SiC}$ = 0.07 and $()d/d)_{SiC}$ = 0.02 in comparison to the value of 3C-SiC) are found at $5x10^{16}$ and $4x10^{17}$ C ions/cm$^2$ and 500°C. They give the increased X-ray intensity detected at the low angle tail of the SiC(111) diffraction line (Fig. 2). By IR absorption studies [9] Si-C pre-stages are identified. The wavenumber of the stretching mode of Si-C bonds starts to

increase before the final SiC crystallization, this is correlated with an increased atomic distance found here.

These particles cause also a small strain of ()d/d)$_{Si}$ = -0.0004 in the Si lattice. This is concluded from the additional intensity which arises near the central substrate peak of Si(400) at its high-angle slope (Fig. 3) in the same samples.

4. Finally, crystalline 3C-SiC particles are found for a fluence of 4x10$^{17}$ C ions/cm$^2$ at 800°C. They are aligned to the Si host lattice in such a way that the cubic crystallographic axes of matrix and particles coincide within an accuracy of 2.5° as it was revealed by RSM studies. The 3C-SiC crystallites are surrounded by an expanded Si lattice (the peak position in Fig. 3 gives ()d/d)$_{Si}$ = 0.0002). The latter may be the consequence of the thermal stress by cooling down the sample from the process to room temperature due to the different coefficients of thermal expansion for Si (3.59x10$^{-6}$ /K) and SiC (4.2 to 4.68x10$^{-6}$ /K), respectively [14]. The SiC lattice itself is strained only negligible (see Fig. 3) if the phase formation occurs during the high-temperature implantation process. This is in contrast to strained SiC particles (($\Delta$d/d)$_{SiC}$ $\approx$ 0.01) which have been reported [15] to form after thermal treatment following room temperature implantation.

Further complex X-ray studies including reciprocal space mapping and texture analysis will enlighten the mechanisms of the formation of SiC precipitates and their state in the Si host lattice.

## References


[1] I. Ban, M.C. Ötztürk and E. Demirlioglu, Proc. of the 11$^{th}$ Int. Conf. on Ion Implantation Technology, Austin, 1996, IEEE Publications 96TH8182, Piscataway, NJ, p. 740

[2] S. Nishikawa, A. Tanaka and T. Yamaji, Appl. Phys. Lett. 60, 2270 (1992)

[3] R. Liefting, R.C.M. Wijburg, J.S. Custer, H. Wallinga and F. Saris, IEEE Transactions on Electron. Devices Vol. 41 No.1 , 50 (1994)

[4] H. Wong, N. W. Cheung, P. K. Chu, J. Liu and J. W. Mayer, Appl. Phys. Lett. 52, 1023 (1988)

[5] U. Preckwinkel, J. K. N. Lindner, B. Stritzker, B. Rauschenbach, Nucl. Instrum. Methods Phys. Res. B 120, 125 (1996)

[6] A. Nejim, P. I. E. Hemment, J. Stoemenos, Appl. Phys. Lett. 66, 2646 (1995)

[7] J. A. Borders, S. T. Picraux, W. Beezhold, Appl. Phys. Lett. 18, 509 (1971)

[8] U. Gösele, Mat. Res. Soc. Symp. Proc. 59, 419 (1985)

[9] M. Deguchi, M. Kitabatake, T. Hirao, N. Arai, T. Izumi, Jap. J. Appl. Phys. 31, 343 (1992)

[10] P. Werner, S. Eichler, G. Mariani, R. Kögler, W. Skorupa, Appl. Phys. Lett. 70, 252 (1997)

[11] T. B. Massalski, Binary Alloy Phase Diagrams, Vol.1, p. 882, ASM International, Ohio 1990

[12] W. Matz, N. Schell, G. Bernhard, F. Prokert, T. Reich, J. Claußner, W. Oehme, R. Schlenk, S. Dienel, H. Funke, F. Eichhorn, M. Betzl, D. Pröhl, U. Strauch, G. Hüttig, H. Krug, W. Neumann, V. Brendler, P. Reichel, M.A. Denecke, H. Nitsche, J. Synchrotron Rad. 6 (1999) in press

[13] computer code WIN-HRXRD, vers.1.02; Siemens 1994

[14] Landoldt-Börnstein, ed. by O. Madelung, Springer, New York 1982, Vol. 17

[15] C. Serre, A. Perez-Rodriguez, A. Romano-Rodriguez, L. Calvo-Barro, J.R. Morante, J. Esteve, M.C. Acero, W. Skorupa and R. Kögler, J. Electrochem. Soc. 144 (6), 2211 (1997)